Experimental Section

Single-Crystal X-ray Diffraction analysis.

Cystallographic data of Ni7Me was collected on a Bruker APEX-II CCD diffractometer equipped with graphite-monochromated Mo Kα radiation (λ = 0.71073 Å) at the room temperature. By using Olex2 software, the structures were solved by direct methods and subsequently refined by full-matrix least-squares techniques on F^2 employing the SHELX program. Anisotropic refinement was performed for all non-hydrogen atoms, and hydrogen atoms were positioned geometrically and refined isotropically by using a riding model.CCDC:2428761.

Thermogravimetric (TGA) analysis.

The as-synthesized sample Ni7Me was immersed in 7mL deionized water for 72 hours to achieve full solvent exchange. Before the experiment, the sample was dried with filter paper to remove the solvent from the surface. TGA measurements were conducted on a NETZSCH TG 209 thermobalance in a nitrogen atmosphere (20 mL/min), samples of Ni7Me were placed in alumina containers and data were recorded at 10 °C/min from 25 to 800 °C.

IAST adsorption selectivity calculation:

The experimental isotherm data for pure C_2H_2 and C_2H_4 (measured at 273 K) were fitted using a Langmuir-Freundlich (L-F) model:

$$q = \frac{a * b * p^c}{1 + b * P^c} \quad (1)$$

Where q and p are adsorbed amounts and pressures of component i, respectively. Using the pure component isotherm fits, the adsorption selectivity is defined by

$$S_{ads} = \frac{q_1/q_2}{p_1/p_2} \quad (2)$$

Where q_i is the amount of i adsorbed and p_i is the partial pressure of i in the mixture.

We used the following written codes to simulate the adsorption selectivity of C_2H_2/C_2H_4 in Fig. 2:

28 # No. of Pressure Point

y1, y2 # Molar fraction of binary mixture (y1 and y2, y1 + y2 = 1)

1, 2, 3, 4, 5, 6, 7, 8, 9, 10, 20, 30, 40, 50, 60, 70, 80, 90, 100, 101, 102, 103, 104, 105, 106, 107, 108, 109 #The unit is same parameter b, kPa

a1, a2 # fitting parameter Nsat (A1) for both component (Unit: mmol/g)

b1, b2 # fitting parameter b1 for both components (Unit: kPa^{-1})

c1, c2 # fitting parameter c1 for both components

0, 0 # fitting parameter Nsat2(A2) for both component(Unit: mmol/g)

0, 0 # fitting parameter b2 for both components (Unit: kPa^{-1})

1, 1 # fitting parameter c2 for both component

Calculation of breakthrough selectivity

The gas adsorption quantity (qi) is calculated from the breakthrough curve using the following formula:

$$breakthrough\ selectivity = \frac{q_A/y_A}{q_B/y_B} \quad (3)$$

where qi is the adsorption capacity of gas i (mmol/g) and yi is the molar fraction of gas i (i=A, B) in the gas mixture.

The gas adsorption capacity is determined as follows:

$$q_i = \frac{f_i(t_1 - t_0) - f_j \int_{t_0}^{t_1} F_i(t)dt}{22.4 \times M} \quad (4)$$

Where f_i and f_j are the flow rates of gas i and j (mL min^{-1}), respectively; t_0 and t_1 are the initial time and the final time of the experiment (min), respectively; $F_i(t)$ and $F_j(t)$ are the functions of the breakthrough curves of components i and j, respectively, and M is the mass of the adsorbent (g).

The pure alkene volume per volume or weight of materials was obtained by the following equation,

$$V_{Pure} = \frac{f_j \int_{t_0}^{t_1} F_j(t)dt}{M/\rho} \quad \text{(based on volume of adsorbent)} \quad (5)$$

$$V_{Pure} = \frac{f_j \int_{t_0}^{t_1} F_j(t)dt}{M} \quad \text{(based on weight of adsorbent)} \quad (6)$$

where f_j is the flow rate of gas j (alkene) (mL/min), respectively; t_0 and t_1 are the initial time and the final time for only pure gas j being detected (min), respectively; $F_j(t)$ is the function of the breakthrough curve of component j; M is the mass of the adsorbent; ρ is the density of the adsorbent.

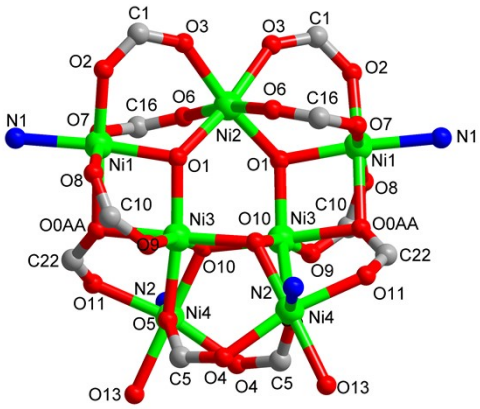

Fig. S1 Metal cluster of Ni7Me

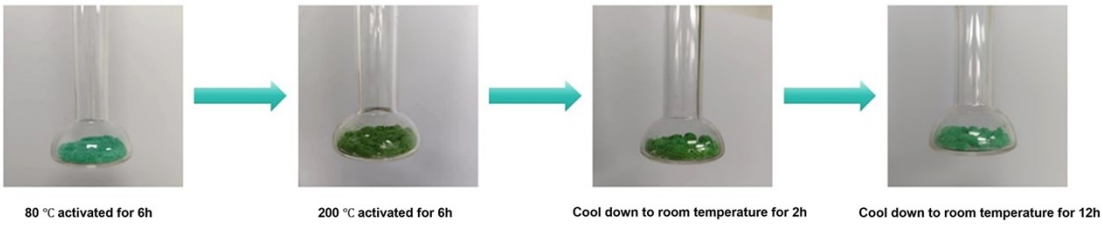

Fig. S2 Pictures of the self-healing process of Ni7Me crystal after heating at 200℃.

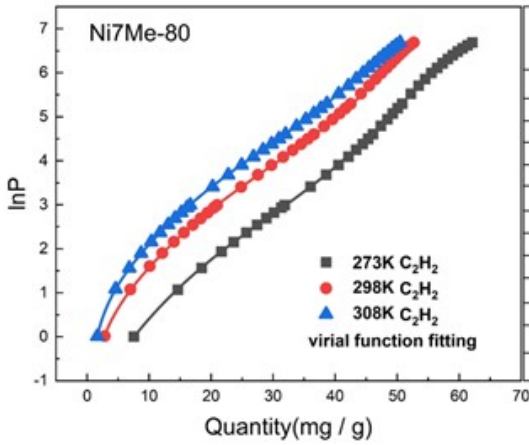

Equation	y=ln(x)+1/k*(a0+a1*x+a2*x^2+a3*x^3+a4*x^4+a5*x^5)+(b0+b1*x+b2*x^2)	
	Value	Standard Error
a0*	-4709.60253	154.40315
a1*	-6.90961	11.37489
a2*	2.0724	0.35336
a3*	-0.09617	0.01106
a4*	0.00181	1.86727E-4
a5*	-1.19053E-5	1.15469E-6
b0*	15.07135	0.51276
b1*	-0.00108	0.03492
b2*	8.09966E-4	5.38931E-4
k	273	0
k	298	0
k	308	0

Fig. S3 The C_2H_2 fit isotherms of Ni7Me-80 at 273 K, 298 K and 308 K by virial equation.

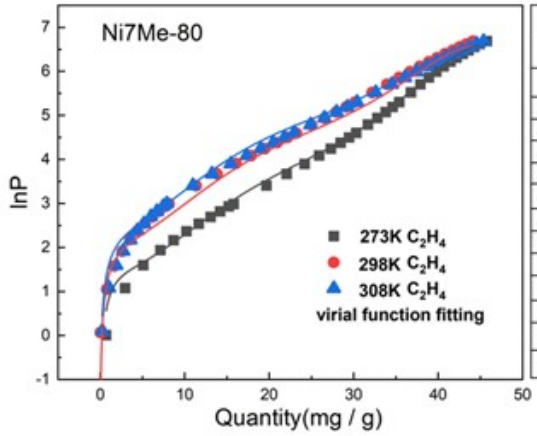

Equation	y=ln(x)+1/k*(a0+a1*x+a2*x^2+a3*x^3+a4*x^4+a5*x^5)+(b0+b1*x+b2*x^2)	
	Value	Standard Error
a0*	-1956.48975	495.57009
a1*	-184.70312	51.39882
a2*	15.30374	2.44933
a3*	-0.61137	0.12561
a4*	0.01339	0.00304
a5*	-1.08344E-4	2.64321E-5
b0*	8.36183	1.68605
b1*	0.25814	0.16721
b2*	-0.00838	0.00342
k	273	0
k	298	0
k	308	0

Fig. S4 The C_2H_4 fit isotherms of Ni7-100 at 273 K, 298 K and 308 K by virial equation.

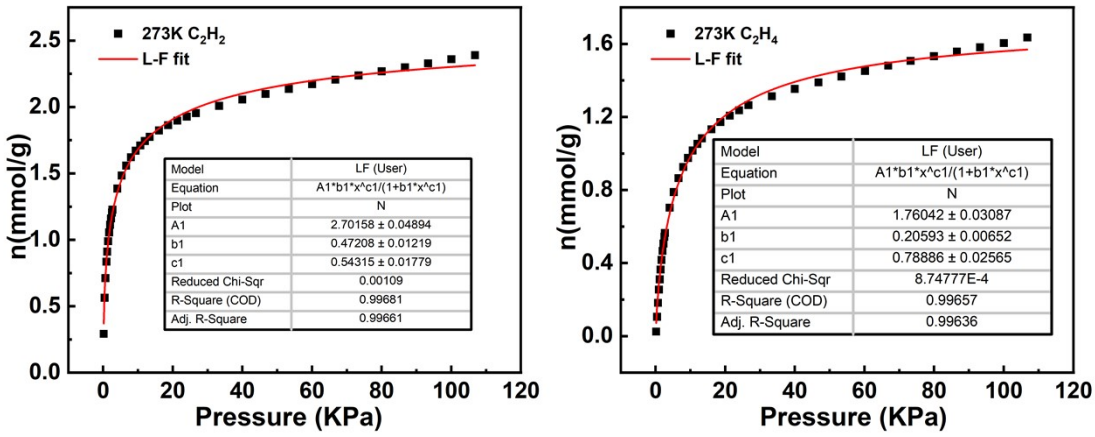

Fig. S5 273 K C_2H_2 and C_2H_4 adsorption isotherm of Ni7Me-80 with fitting by L-F model.

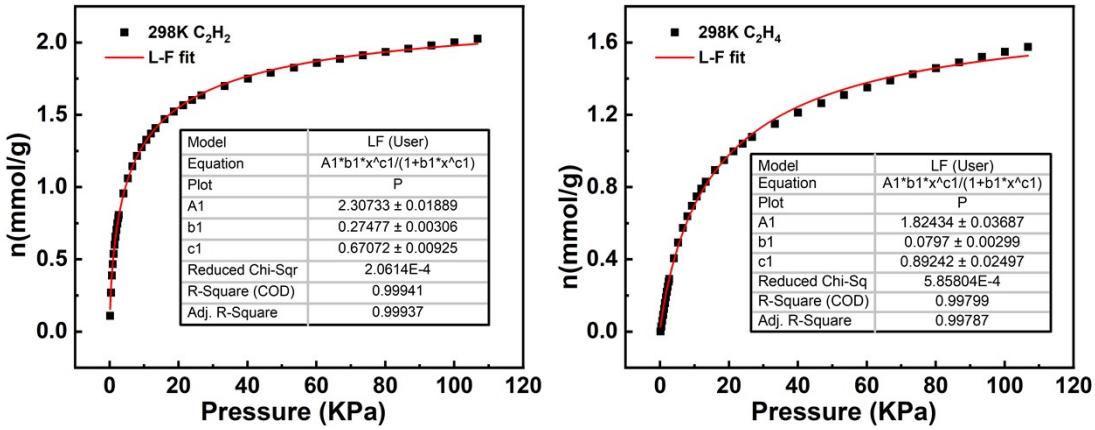

Fig. S6 298 K C_2H_2 and C_2H_4 adsorption isotherm of Ni7Me-80 with fitting by L-F model.

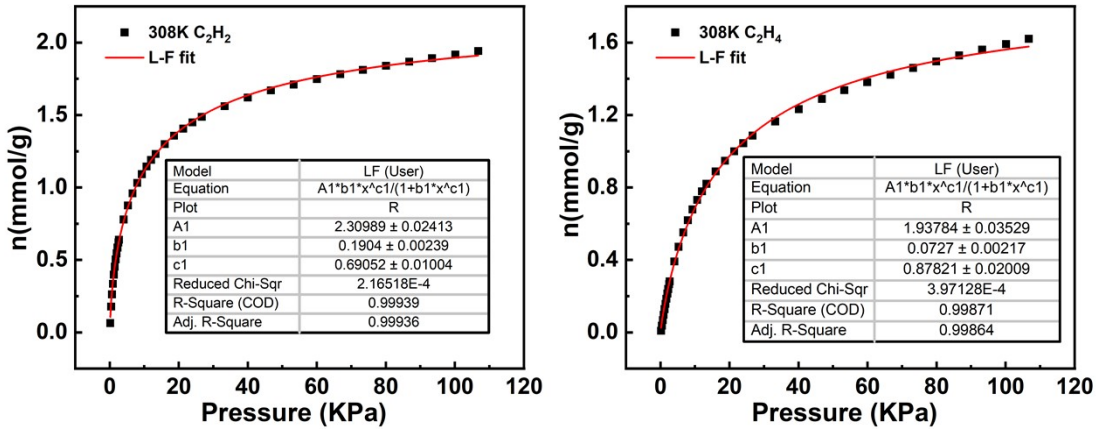

Fig. S7 308 K C_2H_2 and C_2H_4 adsorption isotherm of Ni7Me-80 with fitting by L-F model.

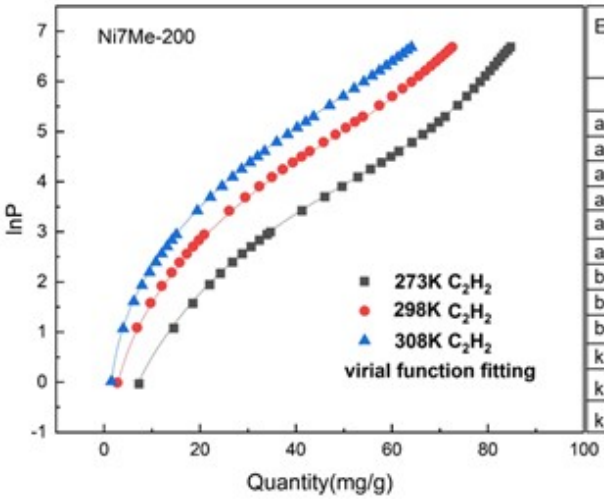

Equation	y=ln(x)+1/k*(a0+a1*x+a2*x^2+a3*x^3+a4*x^4+a5*x^5)+(b0+b1*x+b2*x^2)	
	Value	Standard Error
a0*	-4593.90182	86.60724
a1*	30.36699	5.26728
a2*	-0.19038	0.12854
a3*	-0.01235	0.00308
a4*	1.53662E-4	3.88179E-5
a5*	-5.47377E-7	1.78232E-7
b0*	14.46048	0.51276
b1*	-0.0616	0.01609
b2*	0.00177	1.98004E-4
k	273	0
k	298	0
k	308	0

Fig. S8 The C_2H_2 fit isotherms of Ni7Me-200 at 273 K, 298 K and 308 K by virial equation.

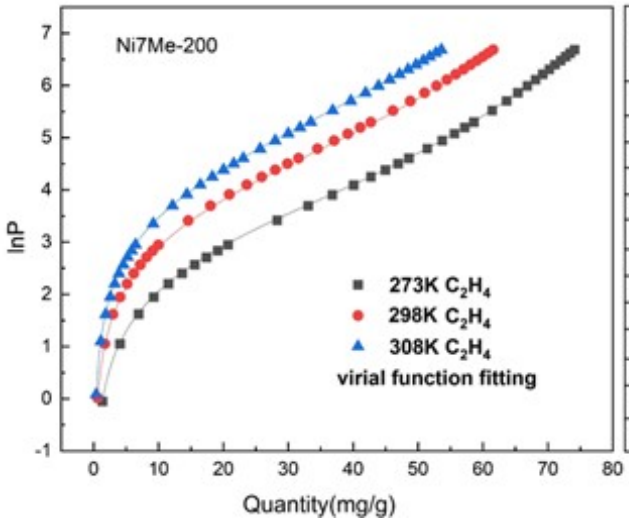

Equation	y=ln(x)+1/k*(a0+a1*x+a2*x^2+a3*x^3+a4*x^4+a5*x^5)+(b0+b1*x+b2*x^2)	
	Value	Standard Error
a0*	-3276.37824	47.26535
a1*	-10.41414	3.99132
a2*	-0.03519	0.11337
a3*	-0.00688	0.00349
a4*	1.17045E-4	5.23471E-5
a5*	-5.8448E-7	2.8164E-7
b0*	11.64294	0.15798
b1*	0.04323	0.01298
b2*	9.42909E-4	2.10472E-4
k	273	0
k	298	0
k	308	0

Fig. S9 The C_2H_4 fit isotherms of Ni7Me-200 at 273 K, 298 K and 308 K by virial equation.

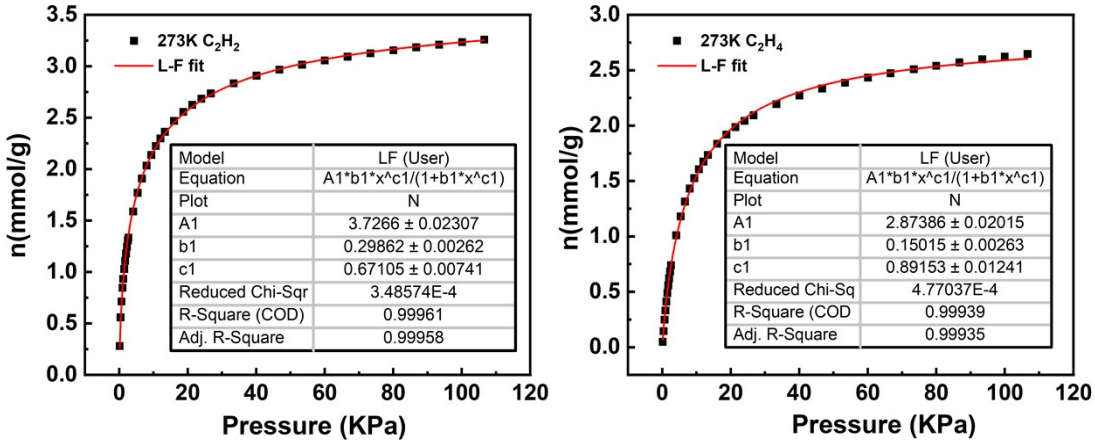

Fig. S10 273 K C_2H_2 and C_2H_4 adsorption isotherm of Ni7Me-200 with fitting by L-F model.

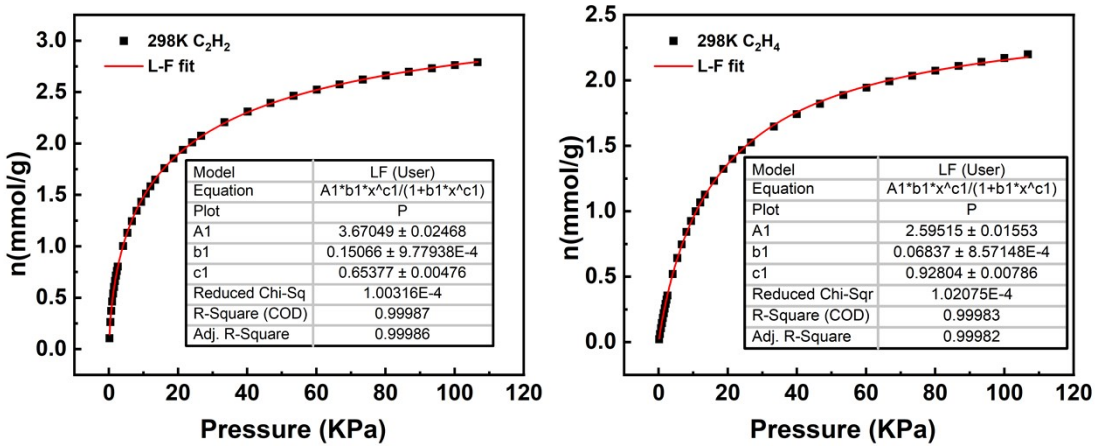

Fig. S11 298 K C_2H_2 and C_2H_4 adsorption isotherm of Ni7Me-200 with fitting by L-F model.

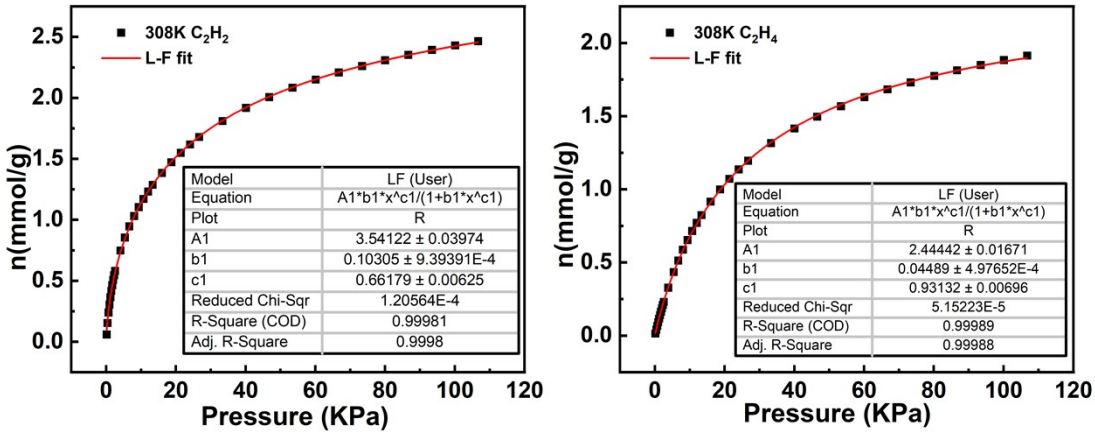

Fig. S12 308 K C_2H_2 and C_2H_4 adsorption isotherm of Ni7Me-200 with fitting by L-F model.

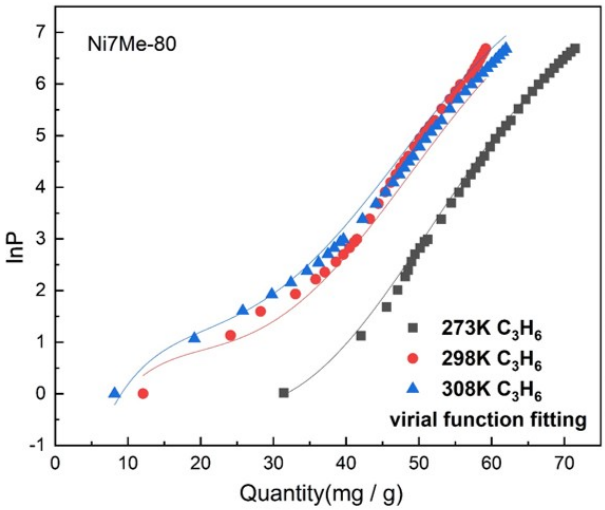

Equation	y=ln(x)+1/k*(a0+a1*x+a2*x^2+a3*x^3+a4*x^4+a5*x^5)+(b0+b1*x+b2*x^2)	
	Value	Standard Error
a0*	1505.19435	3974.65739
a1*	-218.43549	197.12666
a2*	-5.13852	5.67125
a3*	0.25446	0.14082
a4*	-0.00297	0.00178
a5*	1.21339E-5	8.52346E-6
b0*	-9.38944	12.63852
b1*	1.16325	0.53525
b2*	-0.01223	0.0056
k	273	0
k	298	0
k	308	0

Fig. S13 The C_3H_6 fit isotherms of Ni7Me-80 at 273 K, 298 K and 308 K by virial equation.

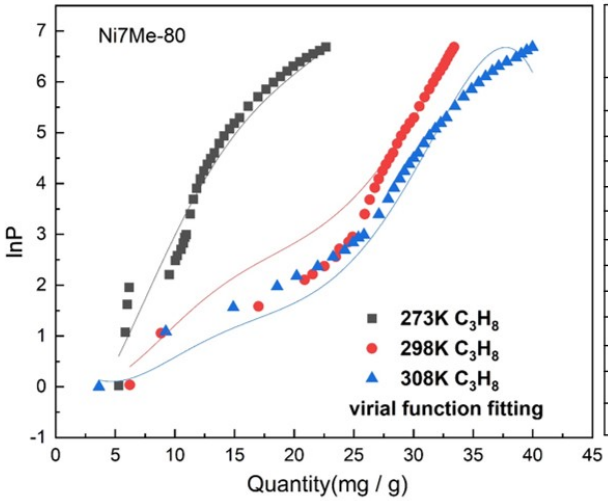

Equation	y=ln(x)+1/k*(a0+a1*x+a2*x^2+a3*x^3+a4*x^4+a5*x^5)+(b0+b1*x+b2*x^2)	
	Value	Standard Error
a0*	-4889.62053	1764.76932
a1*	1161.97683	269.1706
a2*	9.11059	18.25174
a3*	-2.52394	0.83477
a4*	0.07064	0.0202
a5*	-7.16391E-4	1.81344E-4
b0*	17.05775	5.44632
b1*	-4.81492	0.64908
b2*	0.10696	0.01797
k	273	0
k	298	0
k	308	0

Fig. S14 The C_3H_8 fit isotherms of Ni7Me-80 at 273 K, 298 K and 308 K by virial equation.

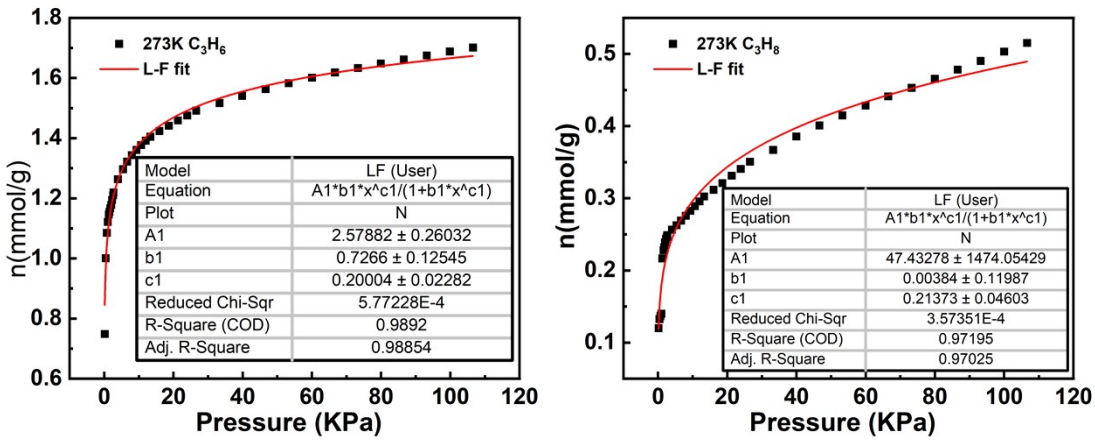

Fig. S15 273 K C_3H_6 and C_3H_8 adsorption isotherm of Ni7Me-80 with fitting by L-F model.

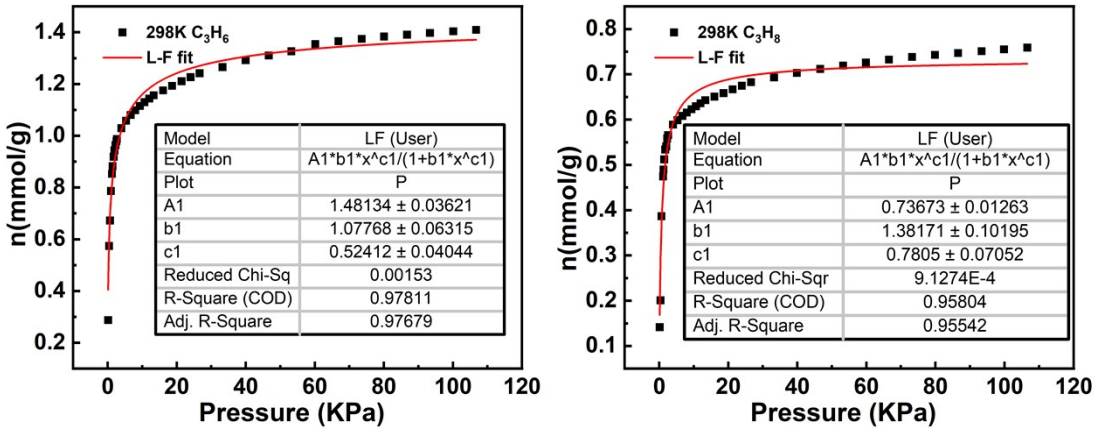

Fig. S16 298 K C_3H_6 and C_3H_8 adsorption isotherm of Ni7Me-80 with fitting by L-F model.

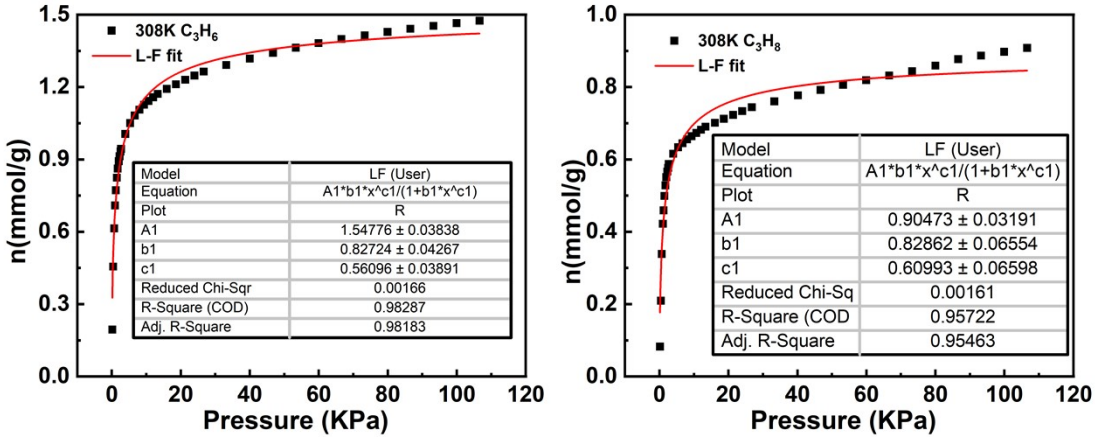

Fig. S17 308 K C_3H_6 and C_3H_8 adsorption isotherm of Ni7Me-80 with fitting by L-F model.

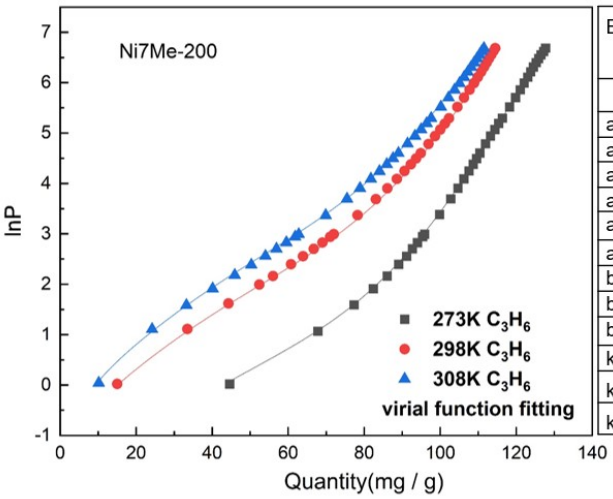

Equation	y=ln(x)+1/k*(a0+a1*x+a2*x^2+a3*x^3+a4*x^4+a5*x^5)+(b0+b1*x+b2*x^2)	
	Value	Standard Error
a0*	-3786.89789	509.24397
a1*	-50.32346	14.45838
a2*	0.96039	0.22624
a3*	-0.01497	0.00327
a4*	1.28278E-4	2.40885E-5
a5*	-3.7894E-7	6.64634E-8
b0*	10.31521	1.64215
b1*	0.11499	0.04136
b2*	-4.12172E-4	2.51799E-4
k	273	0
k	298	0
k	308	0

Fig. S18 The C_3H_6 fit isotherms of Ni7Me-200 at 273 K, 298 K and 308 K by virial equation.

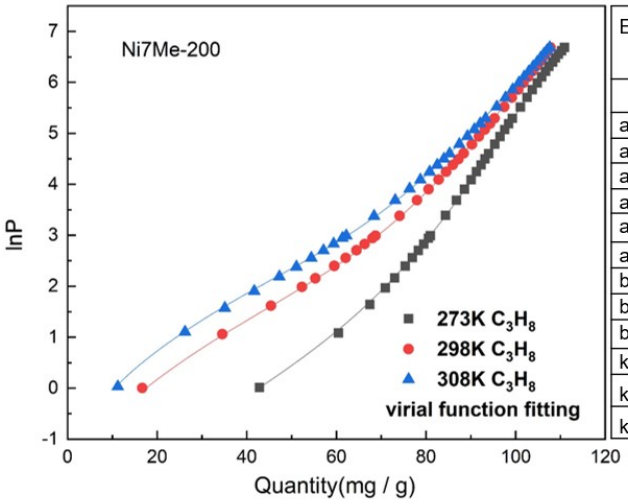

Equation	y=ln(x)+1/k*(a0+a1*x+a2*x^2+a3*x^3+a4*x^4+a5*x^5)+(b0+b1*x+b2*x^2)	
	Value	Standard Error
a0*	-4913.15388	302.47858
a1*	-30.20239	9.75848
a2*	1.25242	0.21498
a3*	-0.01764	0.00363
a4*	1.79922E-4	2.99757E-5
a5*	-6.39768E-7	9.31858E-8
b0*	13.79268	0.95848
b1*	0.05663	0.02463
b2*	-0.00134	1.54166E-4
k	273	0
k	298	0
k	308	0

Fig. S19 The C_3H_8 fit isotherms of Ni7Me-200 at 273 K, 298 K and 308 K by virial equation.

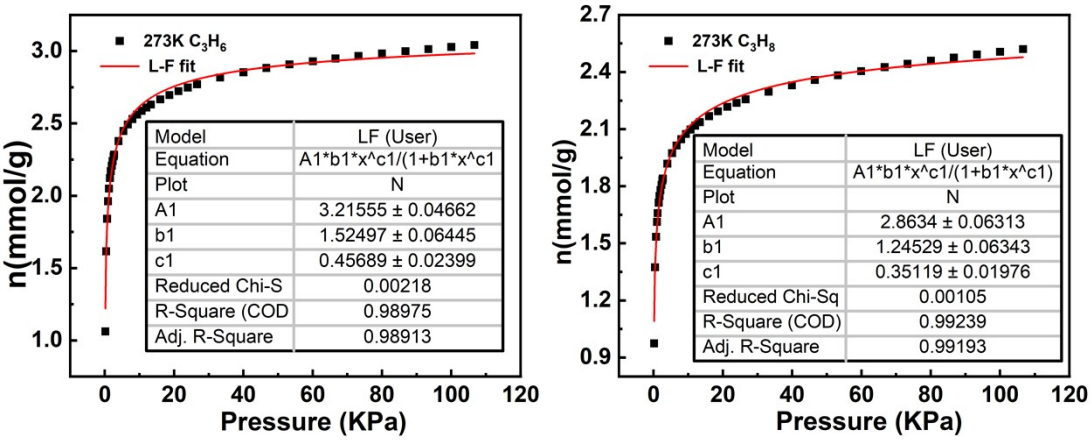

Fig. S20 273 K C_3H_6 and C_3H_8 adsorption isotherm of Ni7Me-200 with fitting by L-F model.

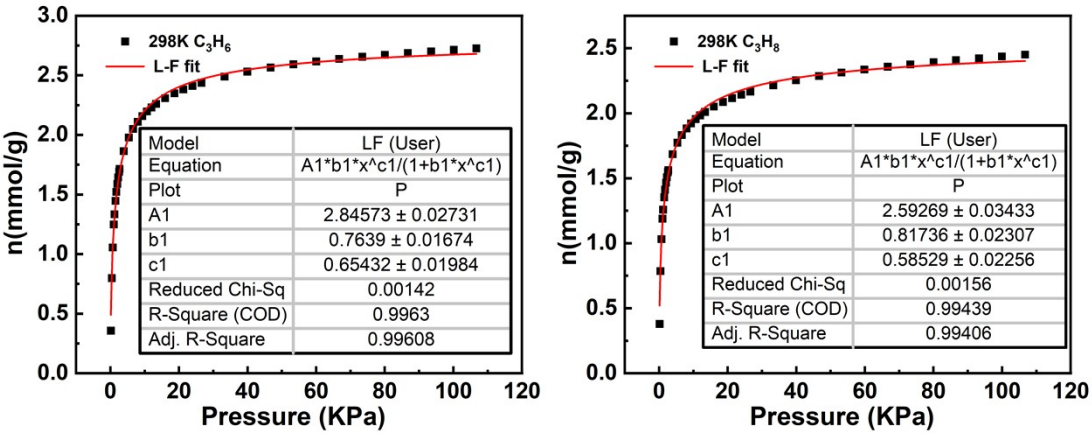

Fig. S21 298 K C_3H_6 and C_3H_8 adsorption isotherm of Ni7Me-200 with fitting by L-F model.

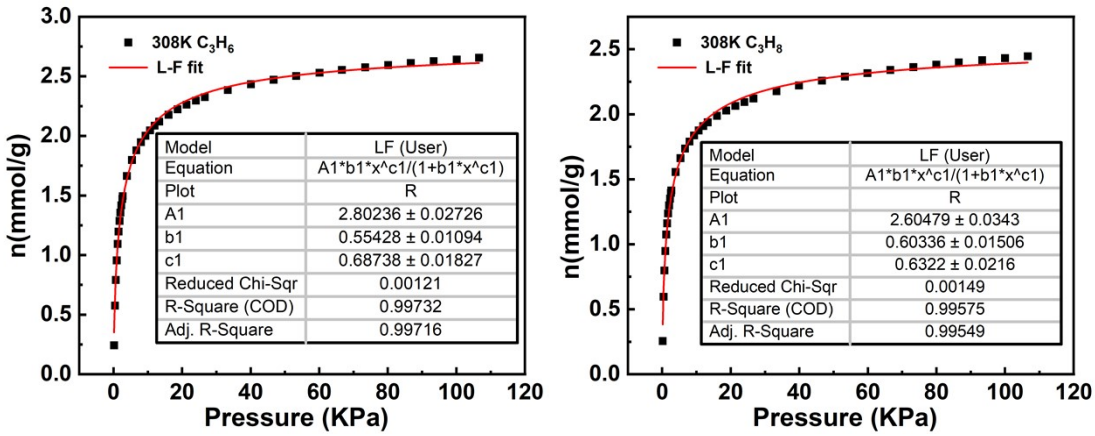

Fig. S22 308 K C_3H_6 and C_3H_8 adsorption isotherm of Ni7Me-200 with fitting by L-F model.

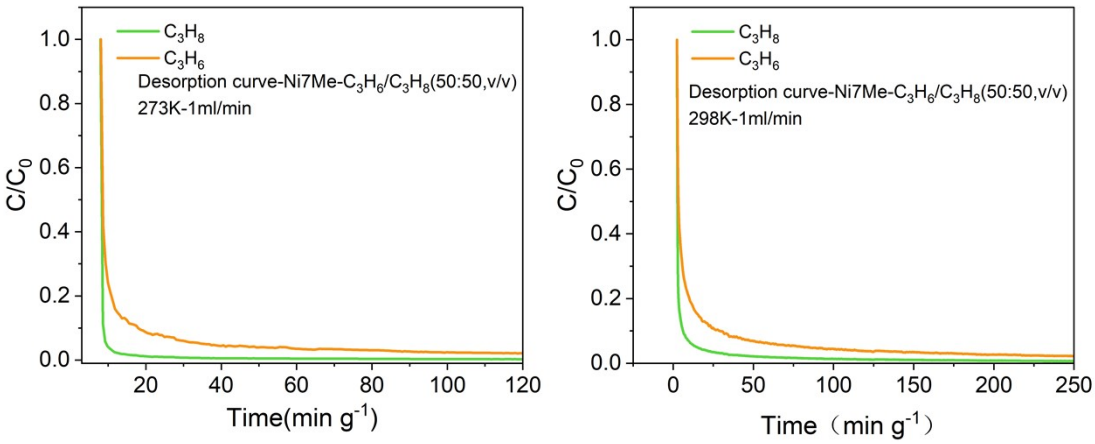

Fig. S23 The gas desorption curve after the penetration test of Ni7Me-80 at 273K and 298K, respectively.

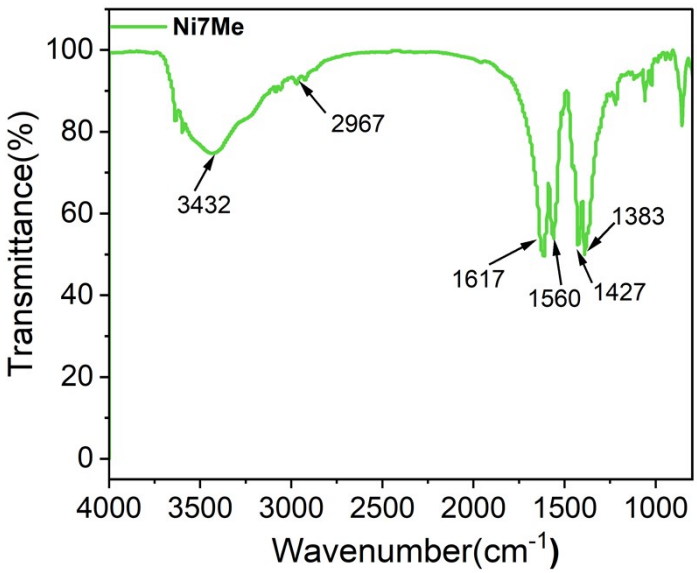

Fig. S24 The infrared spectrum of Ni7Me.

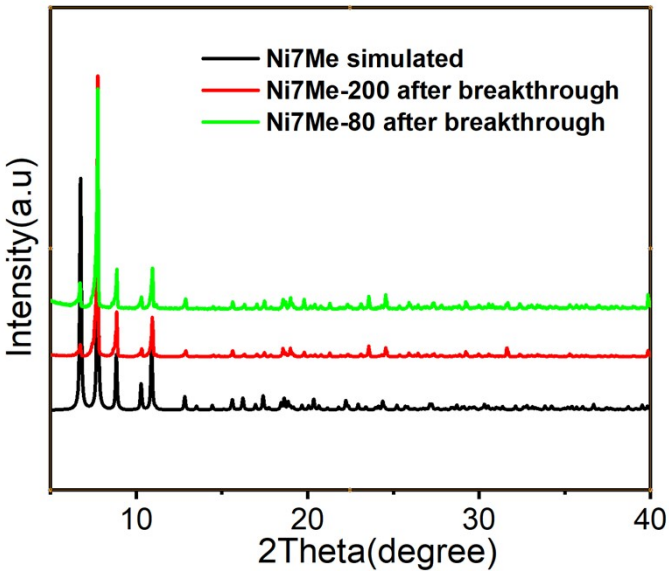

Fig. S25 The XRD patterns of the Ni7Me-80 and Ni7Me-200 after the breakthrough test, respectively.

Table S1 Crystal data and structure refinement for Ni7Me.

Identification code	Ni7Me
Empirical formula	C50H42N4Ni7O26
Formula weight	1525.84
Temperature/K	273.15
Crystal system	Orthorhombic
Space group	Pba2
a/Å	13.721(2)
b/Å	19.762(3)
c/Å	12.978(2)
α/°	90.00
β/°	90.00
γ/°	90.00
Volume/$Å^3$	3519.1(10)
Z	4
ρcalcg/cm^3	1.440
μ/mm^{-1}	1.905
F(000)	1548.0
Crystal size/mm^3	0.1*0.1*0.2
Radiation	MoKα (λ = 0.71073)
2Θ range for data collection/°	4.786 to50.172
Index ranges	$-16 \leq h \leq 16$, $-23 \leq k \leq 23$, $-14 \leq l \leq 15$
Reflections collected	18961
Independent reflections	6109 [Rint = 0.0589, Rsigma = 0.0674]
Data/restraints/parameters	6109/447/412
Goodness-of-fit on F^2	0.999
Final R indexes [I>=2σ (I)]	R1 = 0.0346, wR2 = 0.0725
Final R indexes [all data]	R1 = 0.0457, wR2 = 0.0765
Largest diff. peak/hole / e $Å^{-3}$	0.67/-0.59

Table S2 Selected Bond Lengths (Å) for Ni7-Me MOF.

Ni(1)−O(11)	2.030(8)	Ni(1)−O(10^1)	2.229(9)
Ni(1)−O(1)	1.986(9)	Ni(1)−O(5)	2.164(9)
Ni(1)−O(8^1)	2.123(9)	Ni(1)−N(1^3)	2.116(10)
Ni(2)−O(2)	2.057(9)	Ni(2)−O(11)	2.090(9)
Ni(2)−O(7)	2.065(9)	Ni(4)−O(4^4)	2.162(9)
Ni(3)−O(11)	2.029(9)	Ni(4)−O(12)	2.007(9)
Ni(3)−O(10^1)	2.113(8)	Ni(4)−O(9)	2.132(9)
Ni(3)−O(4^2)	2.126(11)	Ni(4)−N(2^5)	2.122(10)
Ni(3)−O(12^1)	2.129(8)	Ni(4)−O(3^2)	2.079(9)
Ni(3)−O(12)	2.058(9)	Ni(4)−O(13)	2.162(13)
Ni(3)−O(6)	2.057(9)		

[1]1-X,1-Y,+Z; [2]+X,+Y,-1+Z; [3]1/2-X,1/2+Y,+Z; [4]1-X,1-Y,-1+Z; [5]-1/2+X,1/2-Y,+Z

Table S3 C_2H_2 adsorption capacity and C_2H_2 selectivity with other benchmark materials with similar BET surface areas.

MOF	S_{BET} ($m^2 g^{-1}$)	uptake($cm^3 g^{-1}$)		Q_{st}(kJ mol^{-1})		selectivity for C_2H_2/C_2H_4	Ref.
		C_2H_2	C_2H_4	C_2H_2	C_2H_4		
Ni7Me-80	284	45.39	35.29	39.16	16.27	6.08	This work
Ni7Me -200	325	62.50	49.25	38.19	27.24	3.33	This work
BSF-1	535	52.6	36.6	31.0	26	2.3	1
MUF-17	247	67.0[a]	48.0[a]	49.5	31.1	8.7	2
BSF-3	458	80.42	53.09	42.7	28.1	8.0	3
SNNU-333-Ni	519	51.2	27.5	33.8	32.3	4.4	4
NUM-11	374.2	50.5	35.8	18.2	18	1.6[b]	5
JCM-1	550	75	35	36.9	34.2	13.2	6
Cu(bpy)NP	459	50.7	40.8	40.8	31.3	28.5[b]	7
NUM-15a	721.65	78	55.14	37.4	33.2	2.4[b]	8
Zn-atz-oba	710.7	62.048	45.47	27.5	27	1.43	9
UPC-80	431	77.28	50.44	20.84	17.64	4.78	10
UPC-22	486.3	37.4	24.2	21.1	15.9	2.6[b]	11
$Zn(sdba)(dabco)_{0.5}$	224	74.14	60.03	32.45	27.94	1.72[c]	12
NUM-9a	330	52.1	49.9	35.8	32.3	1.5[d]	13
Cu(OH)INA	206	48.3	31.8	36.1	29.6	41[b]	14
FJUT-1	1240	133.2	106.5	43.75	31.01	4.07[b]	15

[a] Gas uptake at 293 K. [b] C_2H_2/C_2H_4 = 1/99. [c] C_2H_2/C_2H_4 = 50/50. [d] Gas uptake at 313 K.

Table S4 C_3H_6 adsorption capacity and C_3H_6 selectivity with other benchmark materials with similar BET surface areas.

MOF	S_{BET} ($m^2 g^{-1}$)	uptake($cm^3 g^{-1}$)		Q_{st} (kJ mol^{-1})	selectivity for C_3H_6/C_3H_8 (50/50)	Ref.
		C_3H_6	C_3H_8	C_3H_6		
Ni7Me -80	284	31.57	17.0	-	71.44	This work
Ni7Me -200	325	61.06	54.89	31.48	1.38	This work
Co-gallate.	486.8	40.07	3.13	41	333	16
MAF-23-O	-	30.2	22.4	78	8.8	17
HIAM-402	1442	138	133.3	31.2	1.43	18
BFFOUR-Cu-dpds	140	27.33	1.90	31.13	8.76	19
$Zn_2(BDC\text{-}Cl)_2(Py_2TTZ)$	441[a]	74.4[a]	36.2[a]	2.5	5.2[a]	20
$Mg_2(dobdc)$	1797[b]	188.16[b]	158.4[b]	46	7.5[b]	21

Cu-BTC	338[b]	141.12[b]	112[b]	50	6.1[b]	22
Zu-36-Ni	246	44.8	11.2	42	1.8	23
GeFSIX-2-Cu-i	467	60.26	40.31	36.5	4	24
SiFSIX-2-Cu-i	503	59.36	37.41	37	4.5	24
CPL-1	330[a]	39.87[a]	6.72[a]	-	2.08[a]	25
Fe_2(m-dobdc)	-	163.74	132.6	73	60	26
Cu-ASY	235	27.1	26.12	-	1.44[c]	27
DL-mal-MOF	380	37.6	27.10	64.4	62.6	28
ZJU-75a	391	74.08[d]	52.2[d]	65.9	54.2[d]	29
Ni-NP	-	79.6	47.7	-	10.5	30

[a] Gas uptake at 273 K. [b] Gas uptake at 318 K. [c] selectivity for C_3H_8/C_3H_6 [d] Gas uptake at 296 K.

Reference:

(1) Y. Zhang, L. Yang, L. Wang, S. Duttwyler, H. Xing, A Microporous Metal-Organic Framework Supramolecularly Assembled from a Cu^{II} Dodecaborate Cluster Complex for Selective Gas Separation, *Angew. Chem. Int. Ed.*, **2019,** *58,* 8145-8150.

(2) O. T. Qazvini, R. Babarao, S. G. Telfer, Multipurpose Metal-Organic Framework for the Adsorption of Acetylene: Ethylene Purification and Carbon Dioxide Removal, *Chem. Mater.,* **2019,** *31*, 4919-4926.

(3) Y. B. Zhang, J. B. Hu, R. Krishna, L. Y. Wang, L. F. Yang, X. L. Cui, S. Duttwyler and H. B. Xing, Rational Design of Microporous MOFs with Anionic Boron Cluster Functionality and Cooperative Dihydrogen Binding Sites for Highly Selective Capture of Acetylene, *Angew. Chem. Int. Ed.,* **2020**, 59, 17664 – 17669

(4) J. Zhang, Y. Y. Xue, P. Zhang, H. P. Li, Y. Wang, J. Xu, S. N. Li, and Q. G. Zhai, Honeycomb-Like Pillar-Layered Metal−Organic Frameworks with Dual Porosity for Efficient C_2H_2/CO_2 and C_2H_2/C_2H_4 Separations, *Cryst. Growth Des.*, **2022**, 22, 469−477

(5) S. Q. Yang, L. Zhou, Y. He, R. Krishna, Q. Zhang, Y. F. An, B. Xing, Y. H. Zhang, and T. L. Hu, Two-Dimensional Metal−Organic Framework with Ultrahigh Water Stability for Separation of Acetylene from Carbon Dioxide and Ethylene, *ACS Appl. Mater. Interfaces,* **2022**, *14,* 33429-33437.

(6) J. Lee, C. Y. Chuah, J. Kim, Y. Kim, N. Ko, Y. Seo, K. Kim, T. H. Bae, and E. Lee, Separation of Acetylene from Carbon Dioxide and Ethylene by a Water-Stable Microporous Metal–Organic Framework with Aligned Imidazolium Groups inside the Channels, *Angew. Chem. Int. Ed.*, **2018**, 57, 7869 –7873

(7) Y. Liu, J. H. Liu, H. T. Xiong, J. W. Chen, S. X. Chen, Z. L. Zeng, S. G. Deng and J. Wang, Negative electrostatic potentials in a Hofmann-type metal-organic framework for efficient acetylene separation, *Nature Communications.,* **2022**, 13, 5515

(8) Q. Zhang, L. Zhou, P. Liu, L. Li, S. Q. Yang, Z. F. Li, T. Liang, Integrating tri-mural nanotraps into a microporous metal-organic framework for C_2H_2/CO_2 and C_2H_2/C_2H_4 separation, *Separation and Purification Technology*, **2022**, 296, 121404-121411.

(9) J. W. Cao, S. Mukherjee, T. Pham, Y. Wang, T. Wang, T. Zhang, X. Jiang, H.-J. Tang, K. A. Forrest, B. Space, M. J. Zaworotko, and K. J. Chen, One-step ethylene production from a fourcomponent gas mixture by a single physisorbent, *Nat. Commun.*, **2021**, 12, 6507

(10) C. H. Jiang, C. L. Hao, X. K. Wang, H. Y. Liu, X. F. Wei, H. K. Xu, Z. F. Wang, Y. Ouyang, W. Y. Guo, F. N. Dai, D. F. Sun, Constructing C_2H_2 anchoring traps within MOF interpenetration nets as C_2H_2/CO_2 and C_2H_2/C_2H_4 bifunctional separator, *Chemical Engineering Journal*, **2023**, 453, 139713

(11) X. P. Liu, Y. Li, C. L. Hao, W. D. Fan, W. Liu, J. Q. Liu, and Y. J. Wang, Optimizing the pore space of a robust nickel-organic framework for efficient C_2H_2/C_2H_4 separation, *Inorg. Chem. Front.,* **2023,** *10,* 824-831.

(12) H. Shuai, J. H. Liu, Y. S. Teng, X. Liu, L. M. Wang, H. T. Xiong, P. X. Wang, J. W. Chen, S. X. Chen, Z. Y. Zhou, S. G. Deng, J. Wang, Pillar-layered metal-organic frameworks with benchmark C2H2/C2H4 and C2H6/C2H4 selectivity for one-step C2H4 production, *Separation and Purification Technology.,* **2023**, 323, 124392

(13) S. Q. Yang, F. Z. Sun, P. Liu, L. Li, R. Krishna, Y. H. Zhang, Q. Li, L. Zhou, T. L. Hu, Efficient Purification of Ethylene from C2 Hydrocarbons with an C_2H_6/C_2H_2-Selective Metal-Organic Framework, *ACS Appl. Mater. Interfaces,* **2021,** *13,* 962-969.

(14) X. Zhang, Q. C. Chen, X. F. Bai, Y. L. Zhao, J. R. Li, Achieving Record C_2H_2 Packing Density for Highly Efficient C_2H_2/C_2H_4 Separation with a Metal-Organic Framework Prepared by a Scalable Synthesis in Water, *Angew. Chem. Int. Ed.,* **2024**, e202411744

(15) L. Zhang, T. T. Xiao, X. Y. Zeng, J. J. You, Z. Y. He, C. X. Chen, Q. T. Wang, A. Nafady, A. M. Al-Enizi, and S. Q. Ma, Isoreticular Contraction of Cage-like Metal–Organic Frameworks with Optimized Pore Space for Enhanced C_2H_2/CO_2 and C_2H_2/C_2H_4 Separations, *J. Am. Chem. Soc.,* **2024**, 146, 11, 7341–7351.

(16) B. Liang, X. Zhang, Y. Xie, R. B. Lin, R. Krishna, H. Cui, Z. Li, Y. Shi, H. Wu, W. Zhou, B. Chen, An

Ultramicroporous Metal–Organic Framework for High Sieving Separation of Propylene from Propane, *J. Am. Chem. Soc.,* **2020**, 142, 17795-17801.

(17) Y. Wang, N. Y. Huang, X. W. Zhang, H. He, R. K. Huang, Z. M. Ye, Y. Li, D. D. Zhou, P. Q. Liao, X. M. Chen, and J.-P. Zhang, Selective Aerobic Oxidation of a Metal–Organic Framework Boosts Thermodynamic and Kinetic Propylene/Propane Selectivity, *Angew. Chem. Int. Ed.,* **2019**, 58, 7692 –7696

(18) X. Y. Li, J. Q. Liu, K. Zhou, S. Ullah, H. Wang, J. Z. Zou, T. Thonhauser, and J. Li, Tuning Metal−Organic Framework (MOF) Topology by Regulating Ligand and Secondary Building Unit (SBU) Geometry: Structures Built on 8-Connected M6 (M = Zr, Y) Clusters and a Flexible Tetracarboxylate for Propane-Selective Propane/Propylene Separation, *J. Am. Chem. Soc.,* **2022**, 144, 21702−21709

(19) Y. Peng, H. T. Xiong, P. X. Zhang, Z. W. Zhao, X. Liu, S. H. Tang, Y. Liu, Z. L. Zhu, W. Z. Zhou, Z. N. Deng, J. H. Liu, Y. Zhong, Z. L. Wu, J. W. Chen, Z. Y. Zhou, S. X. Chen, S. G. Deng and J. Wang, Interaction-selective molecular sieving adsorbent for direct separation of ethylene from senary C2-C4 olefin/paraffin mixture, *Nature Communications.,* **2024**, 15, 625

(20) T. Liu, H. Cui, X. Zhang, Z. Y. Zhang, R. B. Lin, B. Liang, J. Zhang, D. Li, B., Chen Doubly Interpenetrated Metal Organic Framework of pcu Topology for Selective Separation of Propylene from Propane, *ACS Appl Mater Inter.,* **2020**, 12, 48712-48717.

(21) Y. He, R. Krishna, B. Chen, Metal–organic frameworks with potential for energy-efficient adsorptive separation of light hydrocarbons, *Energy Environ. Sci.,* **2012**, 5, 9107-9120.

(22) A. Ferreira, J. Santos, M. Plaza, N. Lamia, J. Loureiro, A. Rodrigues, Suitability of Cu-BTC extrudates for propane–propylene separation by adsorption processes, *Chem. Eng. J.,* **2011**, 167, 1-12.

(23) Z. Zhang, Q. Ding, X. Cui, X. M. Jiang, H. Xing, Fine-Tuning and Selective-Binding within an Anion-Functionalized Ultramicroporous Metal–Organic Framework for Efficient Olefin/Paraffin Separation, *ACS Appl Mater Inter*, **2020**, 12, 40229-40235.

(24) X. Wang, P. Zhang, Z. Zhang, L. Yang, Q. Ding, X. Cui, J. Wang, H. Xing, Efficient Separation of Propene and Propane Using Anion-Pillared Metal–Organic Frameworks, Ind. Eng. Chem. Res., **2020**, 59, 3531-3537.

(25) Y. Chen, Z. Qiao, D. Lv, C. Duan, X. Sun, H. Wu, R. Shi, Q. Xia, Z. Li, Efficient adsorptive

separation of C3H6 over C3H8 on flexible and thermoresponsive CPL-1, *Chem. Eng. J.,* **2017**, 328, 360-367.

(26) J. Bachman, M. Kapelewski, D. Reed, M. Gonzalez, J. Long, M2(m-dobdc) (M = Mn, Fe, Co, Ni) Metal Organic Frameworks as Highly Selective, High-Capacity Adsorbents for Olefin/Paraffin Separations, *J. Am. Chem. Soc.,* **2017**, 139, 15363-15370.

(27) W. Gong, Y. Xie, A. Yamano, S. Ito, E. W. Reinheimer, J. Q. Dong, C. D. Malliakas, D. M. Proserpio, Y. Cui and O. K. Farha, Rational Design and Reticulation of Infinite qbe Rod Secondary Building Units into Metal-Organic Frameworks through a Global Desymmetrization Approach for Inverse C_3H_8/C_3H_6 Separation, *Angew. Chem. Int. Ed.,* **2023**, e202318475.

(28) X. L. Huang, F. Q. Chen, H. R. Sun, L. Yang, Q. W. Yang, Z. G. Zhang, Y. W. Yang, Q. L. Ren, and Z. B. Bao, Quasi-Discrete Pore Engineering via Ligand Racemization in Metal−Organic Frameworks for Thermodynamic−Kinetic Synergistic Separation of Propylene and Propane, *J. Am. Chem. Soc.***,** **2024**, 146, 617−626.

(29) D. Liu, J. Y. Pei, X Zhang, X. W. Gu, H. M. Wen, B. L. Chen, G. D. Qian, and B. Li, Scalable Green Synthesis of Robust Ultra-Microporous Hofmann Clathrate Material with Record C3H6 Storage Density for Efficient C_3H_6/C_3H_8 Separation, *Angew. Chem. Int. Ed.,* **2023**, 62, e202218590

(30) Y. Xie, Y. Shi, H. Cui, R.-B. Lin, B. L. Chen, Efficient Separation of Propylene from Propane in an Ultramicroporous Cyanide-Based Compound with Open Metal Sites, *Small Struct.,* **2022**, 3, 2100125.